captoethanol. The crystals belong to the space group $P2_12_12$ with unit cell dimensions a = 88.5 Å, b = 111.5 Å, and c = 52.9 Å, and there are two yCCS monomers in the asymmetric unit.

Data collection, structural determination and refinement. Crystals were transferred either to precipitant solution containing 20% glycerol or to paratone N oil (Exxon), and flash cooled at -160 °C. Diffraction data were collected at the Dupont-Northwestern-Dow Collaborative Access Team (DND-CAT) beamline at the Advanced Photon Source using a 2k × 2k Mar CCD detector. Data for MAD phasing were collected at three different wavelengths using the reverse beam technique. All data were processed with DENZO and SCALEPACK[27]. The selenium atoms were located by difference Patterson methods and initially refined with the program MLPHARE[28]. The selenium positions were further refined with the CNS program package[29], and an initial electron density map was calculated at 2.5 Å resolution. This map allowed the unambiguous tracing of residues 5–94, 101–199, and 207–218 using the program O (ref. 30). The high-resolution data set (1.8 Å) was then used for further cycles of model building and refinement with CNS. The higher resolution maps allowed the modeling of residues 2–4, 95–100, 200–206, and 219–222 as well as the addition of two sulfate ions and 352 water molecules. The C-terminal 27 residues are disordered and were not modeled. A Ramachandran plot generated with PROCHECK[31] shows that the current model exhibits good geometry with 92.5% of the residues in the most favored regions and 7.5% of the residues in additional allowed regions. Figures were generated using MOLSCRIPT[32] and RASTER3D[33]. The yCCS and ySOD1 dimer interfaces were analyzed using the Protein–Protein Interaction Server (http://www.biochem.ucl.ac.uk/bsm/PP/server).

Coordinates. The coordinates of yCCS have been deposited in the Brookhaven Protein Data Bank (accession code 1qup).

Acknowledgments

We thank L. Pascoli and M. Hou for assistance with crystallization and J. Quintana and D. Keane for assistance with data collection. This work was supported by a grant from the NIH (to A.C.R.), by funds from the ALS Association (A.C.R.), by funds from the Robert H. Lurie Cancer Center (A.C.R.), by a grant from the NIH (to T.V.O.), by a supplement from NIGMS to this same grant (to A.C.R. and T.V.O.), by funds from the ALS Association (T.V.O.), and by an NIH NRSA Training Grant (R.A.P.). The DND-CAT Synchrotron Research Center at the Advanced Photon Sourceis supported by the E.I. Dupont de Nemours & Co., The Dow Chemical Company, the NSF and the State of Illinois.

Correspondence should be addressed to A.C.R. *email: amyr@nwu.edu*

Received 11 March, 1999; accepted 30 April, 1999.

1. Culotta, V.C. *et al. J. Biol. Chem.* **272**, 23469–23472 (1997).
2. Pufahl, R.A. *et al. Science* **278**, 853–856 (1997).
3. Valentine, J.S. & Gralla, E.B. *Science* **278**, 817–818 (1997).
4. Rae, T.D., Schmidt, P.J., Pufahl, R.A., Culotta, V.C. & O'Halloran, T.V. *Science* **284**, 805–808 (1999).
5. Lin, S.-J., Pufahl, R.A., Dancis, A., O'Halloran, T.V. & Culotta, V.C. *J. Biol. Chem.* **272**, 9215–9220 (1997).
6. Gamonet, F. & Lauquin, G.J. *Eur. J. Biochem.* **251**, 716–723 (1998).
7. Glerum, D.M., Shtanko, A. & Tzagoloff, A. *J. Biol. Chem.* **271**, 14504–14509 (1996).
8. Srinivasan, C., Posewitz, M.C., George, G.N. & Winge, D.R. *Biochemistry* **37**, 7572–7577 (1998).
9. Rosenzweig, A.C. *et al. Structure* **7**, 605–617 (1999).
10. Gitschier, J., Moffat, B., Reilly, D., Wood, W.I. & Fairbrother, W.J. *Nature Struct. Biol.* **5**, 47–54 (1998).
11. Steele, R.A. & Opella, S.J. *Biochemistry* **36**, 6885–6895 (1997).
12. Bull, P.C. & Cox, D.W. *Trends Genet.* **10**, 246–252 (1994).
13. Kissinger, C.R., Sieker, L.C., Adman, E.T. & Jensen, L.H. *J. Mol. Biol.* **219**, 693–715 (1993).
14. Portnoy, M.E. *et al. J. Biol. Chem.* **274**, 15041–15045 (1999).
15. Lyons, T.J. *et al. J. Biol. Inorg. Chem.* **3**, 650–662 (1998).
16. Tainer, J.A., Getzoff, E.D., Beem, K.M., Richardson, J.S. & Richardson, D.C. *J. Mol. Biol.* **160**, 181–217 (1982).
17. Getzoff, E.D., Tainer, J.D., Stempien, M.M., Bell, G.I. & Hallewell, R.A. *Proteins* **5**, 322–336 (1989).
18. Bordo, D., Djinovic, K. & Bolognesi, M. *J. Mol. Biol.* **238**, 366–386 (1994).
19. Getzoff, E.D. *et al. Nature* **306**, 287–290 (1983).
20. Djinovic, K. *et al. J. Mol. Biol.* **225**, 791–809 (1992).
21. Jones, S. & Thornton, J.M. *Proc. Natl. Acad. Sci. USA* **93**, 13–20 (1996).
22. Bertini, I., Piccioli, M., Viezzoli, M.S., Chiu, C.Y. & Mullenbach, G.T. *Eur. J. Biophys.* **23**, 167–176 (1994).
23. Stites, W.E. *Chem. Rev.* **97**, 1233–1250 (1997).
24. Valentine, J.S. & Pantoliano, M.W. in *Copper proteins* (ed. Spiro, T.G.) 291–358 (Wiley-Interscience, New York; 1981).
25. Siddique, T., Nijhawan, D. & Hentati, A. *J. Neural Transm.* **49**, 219–233 (1997).
26. Hendrickson, W.A., Horton, J.R. & LeMaster, D.M. *EMBO J.* **9**, 1665–1672 (1990).
27. Otwinowski, Z. & Minor, W. *Methods Enzymol.* **276**, 307–326 (1997).
28. Collaborative Computational Project, Number 4 *Acta Crystallogr.* **D50**, 760–763 (1994).
29. Brünger, A.T. *et al. Acta Crystallogr.* **D54**, 905–921 (1998).
30. Jones, T.A., Zou, J.-Y., Cowan, S.W. & Kjeldgaard, M. *Acta Crystallogr.* **A47**, 110–119 (1991).
31. Laskowski, R.A. *J. Appl. Crystallogr.* **26**, 283–291 (1993).
32. Kraulis, P.J. *J. Appl. Crystallogr.* **24**, 946–950 (1991).
33. Merritt, E.A. & Bacon, D.J. *Methods Enzymol.* **277**, 505–524 (1997)

Solution structure of the homodimeric core domain of *Escherichia coli* histidine kinase EnvZ

Chieri Tomomori[1], Toshiyuki Tanaka[1], Rinku Dutta[2], Heiyoung Park[2], Soumitra K. Saha[2], Yan Zhu[2], Rieko Ishima[3,4], Dingjiang Liu[3,5], Kit I. Tong[3], Hirofumi Kurokawa[3], Hong Qian[3], Masayori Inouye[2] and Mitsuhiko Ikura[3]

[1]Center for Tsukuba Advanced Research Alliance and Institute of Applied Biochemistry, University of Tsukuba, Tsukuba, Ibaraki 305-8577, Japan. [2]Department of Biochemistry, Robert Wood Johnson Medical School, University of Medicine and Dentistry of New Jersey, New Jersey 08854, USA. [3]Division of Molecular and Structural Biology, Ontario Cancer Institute and Department of Medical Biophysics, University of Toronto, Toronto, Ontario M5G 2M9, Canada. [4]Present address: Molecular Structural Biology Unit, National Institute of Dental Research, National Institutes of Health, Bethesda, Maryland 20892, USA. [5]Present address: Schering-Plough Research Institute, Kenilworth, New Jersey 07033-0539, USA.

***Escherichia coli* osmosensor EnvZ is a protein histidine kinase that plays a central role in osmoregulation, a cellular adaptation process involving the His-Asp phosphorelay signal transduction system. Dimerization of the transmembrane protein is essential for its autophosphorylation and phosphorelay signal transduction functions. Here we present the NMR-derived structure of the homodimeric core domain (residues 223–289) of EnvZ that includes His 243, the site of autophosphorylation and phosphate transfer reactions. The structure comprises a four-helix bundle formed by two identical helix-turn-helix subunits, revealing the molecular assembly of two active sites within the dimeric kinase.**

Histidine kinases play a major role in signal transduction that is essential for bacterial stress adaptation[1]. *Escherichia coli* has 32 histidine kinases[2], many of which function as transmembrane signal sensors/transducers in response to specific external sig-

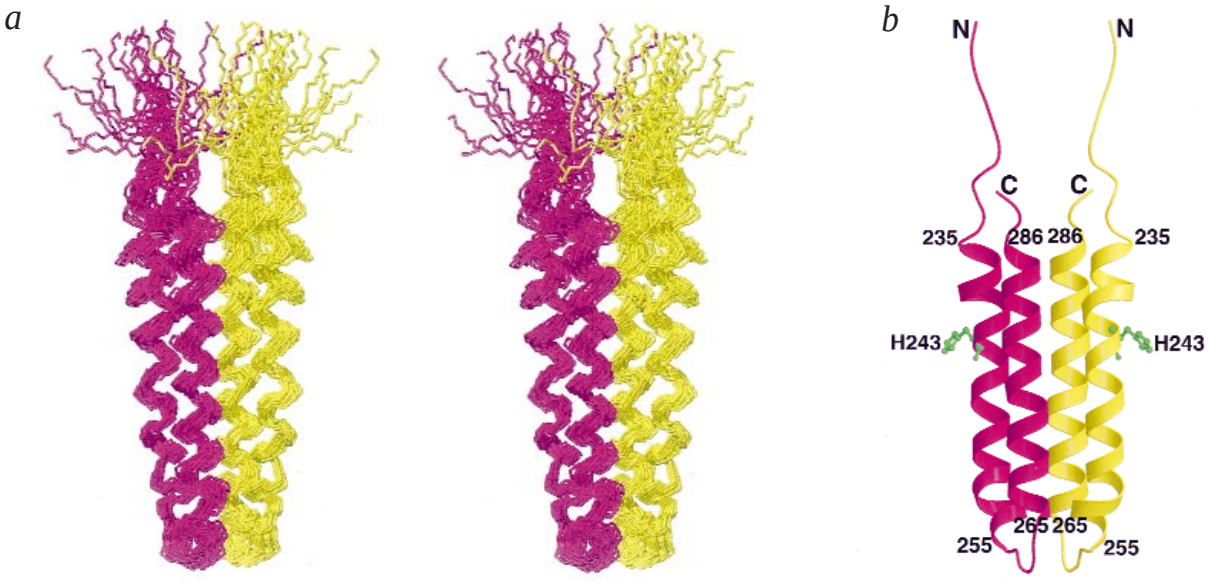

Fig. 1 Three-dimensional structure of EnvZ domain A. ***a***, Stereoview showing a best-fit superposition of the selected 30 NMR-derived structures of EnvZ domain A (residues 223–289). The main chain atoms of the 30 structures are superimposed against the structure with the lowest NOE violations involving residues 235–255 and 265–286. The two identical subunits A and B are colored in pink and yellow, respectively. ***b***, Ribbon diagram of EnvZ domain A. The conserved His 243 is shown as a ball and stick model in green. The residues at the start and end of helices, as well as the N- and C-termini of the protein, are labeled. The color schemes are the same as in Fig. 1*a*.

nals. Some eukaryotes such as yeast and lower plants also possess histidine kinases in addition to serine/threonine and tyrosine kinases[3]. Histidine kinases can be classified into two types based on the location of their substrate His and surrounding residues (H box) with respect to the ATP binding domain, which contains four regions of sequence similarity (G1, G2, F, and N boxes). In type I histidine kinases, the H box is immediately followed by the ATP binding domain, whereas in the type II enzymes, the H box is typically located in the P1 domain at the N-terminus. The regions containing the H box in the two subfamilies have distinct sequences[3].

EnvZ is a transmembrane osmosensor consisting of 450 amino acid residues that encompass all conserved motifs common to the type I histidine kinase subfamily. The kinase/phosphatase domain (residues 223–450) is in the C-terminal cytoplasmic segment and is attached to the transmembrane region through the linker domain (residue 180–222)[4]. The kinase/phosphatase domain of EnvZ exists as a soluble fragment when over-expressed either with or without the linker region[5]. This domain can be further dissected into two functional fragments, domain A (residues 223–289) and domain B (residues 290–450)[6]. Domain A forms a stable homodimer (K_a ~10^5 M^{-1})[7] and contains His 243 in the H box, the autophosphorylation site. Domain B, on the other hand, exists as a monomer in solution and retains ATP binding activity. Neither domain A nor domain B exhibits autophosphorylation activity in isolation. However, His 243 in domain A can be phosphorylated by domain B in the presence of ATP, and this phosphate moiety is transferable to Asp 55 on OmpR[6].

The structural independence and functional complementarity of domains A and B have greatly facilitated the structure determination of EnvZ. Here we report the NMR-derived solution structure of EnvZ domain A, which is essential for dimerization and hence a key structural element in the His-Asp phosphorelay system. The structure reveals that the dimerization core domain comprises a four-helix bundle. We have also investigated the interaction of EnvZ with OmpR using NMR spectroscopy, providing insights into the basis of the specificity of EnvZ–OmpR interaction.

Structure determination

Previous biochemical studies[6,7] demonstrated that domain A of EnvZ forms a stable homodimer with an apparent molecular weight of 19 kDa, as estimated by gel filtration experiments. The ^{1}H-^{15}N heteronuclear single quantum coherence (HSQC) spectrum of this domain displays ~80 highly dispersed peaks in the fingerprint region. This corresponds approximately to the total number of amide protons from the backbone (NH), and from Asn and Gln side chains (NH_2) (domain A contains 67 backbone NHs and 7 side chain NH_2 groups). This observation is consistent with a dimer consisting of two identical subunits exhibiting two-fold symmetry. The linewidth of HSQC peaks indicated that the overall rotational correlation time of this domain (12–14 ns) corresponds to that of a 16–18 kDa globular protein.

The structure of domain A of EnvZ has been determined using multidimensional NMR spectroscopy. To distinguish intra- and inter-subunit NOEs, we used three-dimensional ^{13}C-edited, ^{13}C-filtered NOESY spectra (see ref. 8 for review) using a sample containing a 1:1 mixture of $^{15}N/^{13}C$-labeled and unlabeled proteins. Structure calculations employed simulated annealing protocols with a total of 1,797 experimental NMR restraints, including 27 inter-subunit NOEs. The average pairwise root mean square (r.m.s.) deviation of the NMR-derived structure is 1.10 Å for the backbone atoms and 1.90 Å for all heavy atoms (the N-terminal residues 223–234, the turn between two helices 256–264, and the C-terminal residues 287–289 were unstructured and were not included in this calcu-

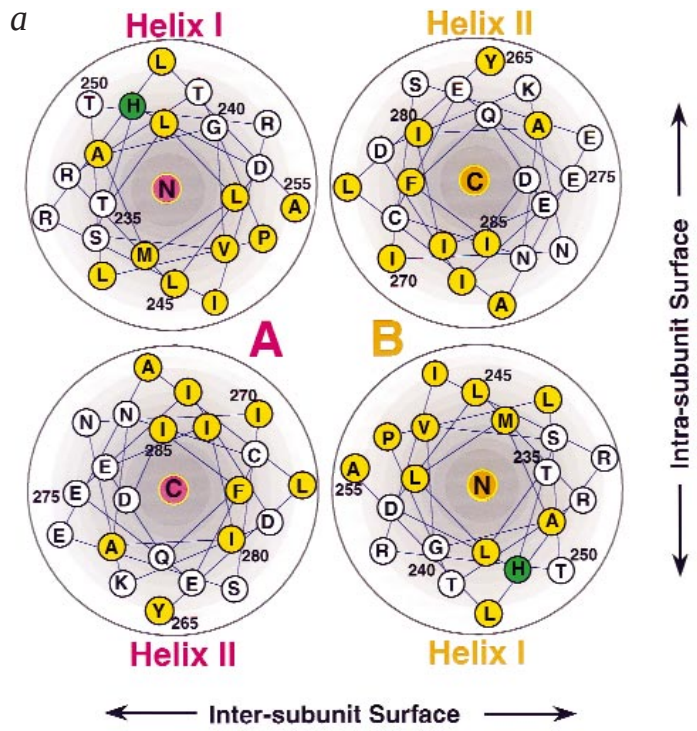

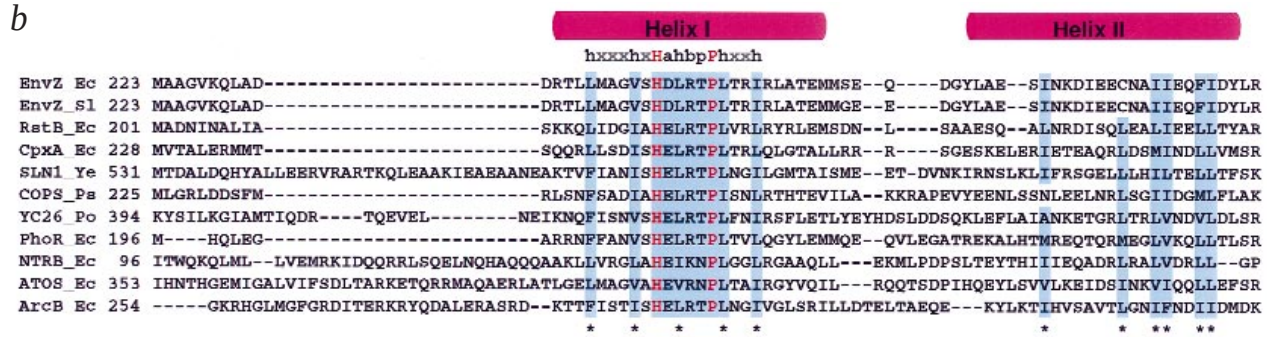

Fig. 2 Hydrophobic core and sequence alignment of EnvZ domain A. ***a***, Helical wheel representation of domain A in projection down the bundle axis. N or C at the center of each wheel indicates which terminus is closer to the reader. Subunits A and B are labeled in the same color scheme as Fig. 1. The hydrophobic residues are shown in yellow, and His 243 (the site of autophosphorylation) in green. ***b***, Sequence alignment of 11 selected histidine kinases for the region corresponding to EnvZ domain A using Ψ-BLAST[31]. The name of each protein is given, followed by the relevant organism: Ec, *E. coli*; Sl, *Salmonella typhimurium*; Ye, *Saccharomyces cerevisiae;* Ps, *Pseudomonas syringae (pv. tomato)*; Po, *Porphyra purpurea* (plant). The accession numbers of the SWISS-PROT protein sequence database are as follows: P02933 (EnvZ_Ec), P08982 (EnvZ_Sl), P18392 (RstB_Ec), P08336 (CpxA_Ec), P39928 (SLN1_Ye), Q02541 (COPS_Ps), P51392 (YC26_Po), P08400 (PhoR_Ec), P06712 (NTRB_Ec), Q06067 (ATOS_Ec) and P22763 (ArcB_Ec). Secondary structure elements determined in the present study are indicated with pink cylinders for α-helices. Conserved hydrophobic residues among histidine kinase family members are marked with an asterisk. A consensus sequence found in helix I is shown at the top of the alignment, and the highly conserved residues are highlighted in cyan.

lation). A summary of the structural statistics is given in Table 1. The superimposed 30 final structures are shown in stereo in Fig. 1*a*.

Structure description

The EnvZ domain A homodimer is a four-helix bundle with a two-fold symmetry along the helical axis. Each subunit folds into a compact structure consisting of antiparallel helices (helix I, residues 235–255; helix II, 265–286) connected by a nine-residue turn (Fig. 1*a*,*b*). The packing of the two identical subunits is schematically illustrated in Fig. 2*a*. The overall dimensions are ~13 Å × 13 Å × 36 Å (when the flexible N-terminal residues 223–234 are omitted). Within the four-helix bundle, residues 242–248 of helix I are somewhat poorly defined (r.m.s. deviation 1.14 Å for the backbone atoms and 1.99 Å for all heavy atoms when calculated with only these residues). Interestingly, this region contains His 243, the site of autophosphorylation and that of phosphorelay to OmpR. This active site is exposed to solvent (Fig. 1*b*).

The four amphipathic helices pack against each other to form a hydrophobic core aligned along their long axes (Fig. 2*a*). Helix I of subunit A interacts intimately with helix II of the same subunit, and with helix II of subunit B, both in an antiparallel manner (interhelical angles are 175° ± 2° and 172° ± 3°, respectively). Consequently, helix I of subunit A and helix I of subunit B are parallel to each other and lie at diagonally opposite corners of the projection down the bundle axis (Fig. 2*a*). The relative arrangement is the same for the two helices II of subunit A and B. The interhelical angles are 12° ± 4° for helix I–helix I, and 5° ± 3° for helix II–helix II in the dimer, respectively. The hydrophobic core consists of numerous methyl-containing residues (Leu 237, Met 238, Val 241, Leu 245, Ile 252, and Ala 255 in helix I; Leu 266, Ile 270, Ile 274, Ile 280, Ile 281, and Ile 285 in helix II from each subunit) and one phenylalanine residue (Phe 284) in helix II. The total surface area buried in the dimer interface is 1,200 ± 120 Å^2 per subunit, which corresponds to 21% of the entire accessible surface area of each subunit (5,700 ± 110 Å^2). A total of 90% of the surface area buried at the dimer interface is hydrophobic in nature.

The structures of two histidine kinase family members, the histidine-containing phosphotransfer domains of CheA (residues 1–134) and ArcB (residues 654–777) have been determined[9,10]. In these structures, both phosphotransfer domains of CheA and ArcB contain multiple helices forming a bundle-like structure with the active His residue (His 48 in CheA and

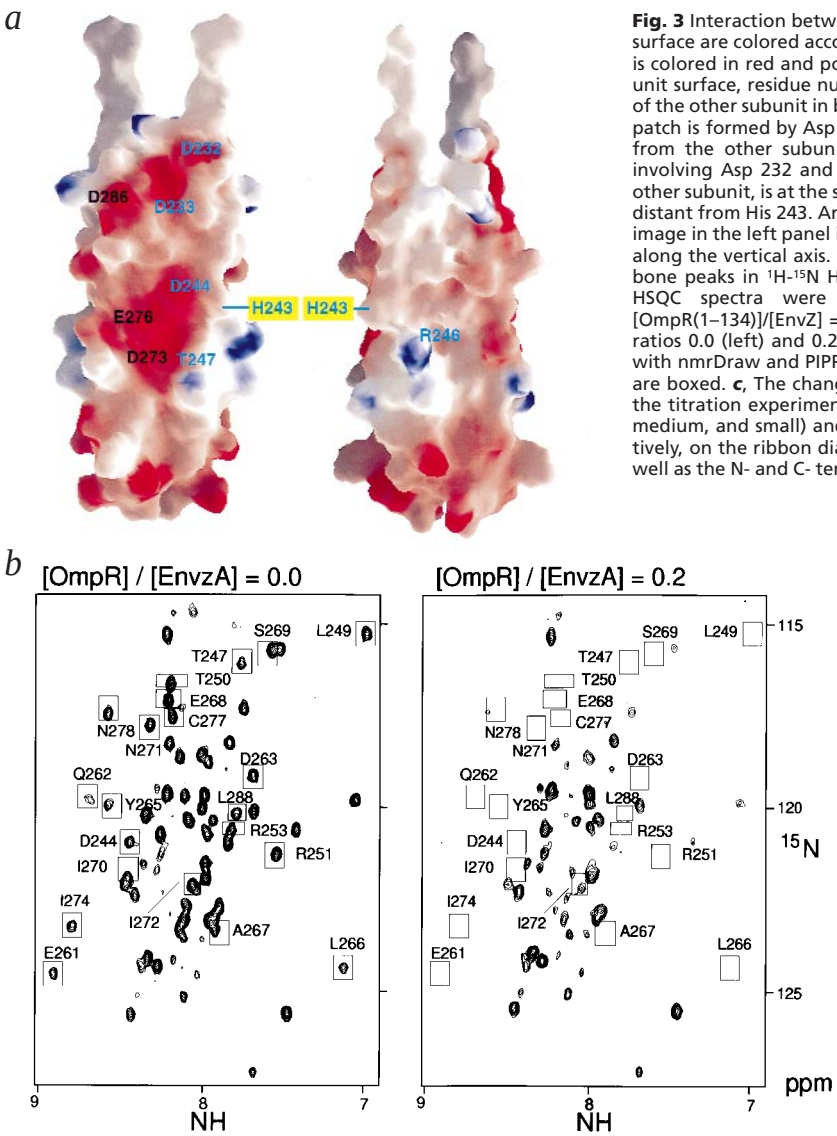

Fig. 3 Interaction between EnvZ and OmpR. ***a***, Two views of the molecular surface are colored according to electrostatic potential. Negative potential is colored in red and positive potential in blue. To highlight the inter-subunit surface, residue numbers of one subunit are shown in blue and those of the other subunit in black. In the vicinity of His 243 and Thr 247, an acidic patch is formed by Asp 244 from one subunit and by Asp 273 and Glu 276 from the other subunit (left hand panel). An additional acidic cluster, involving Asp 232 and Asp 233 from one subunit and Asp 286 from the other subunit, is at the same molecular face as the other acidic cluster, but is distant from His 243. Arg 246 is also close to His 243 (right hand panel). The image in the left panel is related to that in the right panel by a 90° rotation along the vertical axis. ***b***, OmpR-induced changes in intensity of the backbone peaks in ^{1}H-^{15}N HSQC spectra of EnvZ domain A. A series of ^{1}H-^{15}N HSQC spectra were recorded at each of the following ratios: [OmpR(1–134)]/[EnvZ] = 0.0, 0.2, 0.4, 0.6, 0.8, and 1.0. Only the spectra at ratios 0.0 (left) and 0.2 (right) are shown. Peak intensities were analyzed with nmrDraw and PIPP software. Peaks that displayed very large changes are boxed. ***c***, The changes in cross peak intensities in the HSQC spectra in the titration experiment are classified into four groups (very large, large, medium, and small) and shown in red, orange, yellow, and green, respectively, on the ribbon diagram of EnvZ domain A. The conserved His 243 as well as the N- and C- termini are marked.

His 717 in ArcB) located in the middle of helix, analogous to the four-helix bundle of EnvZ. However, it should be noted that both CheA and ArcB phosphotransfer domains exist as asymmetric monomers providing one active His per structural unit, whereas the EnvZ domain A forms a symmetric homodimer providing two active His residues per structural unit. More recently, the crystal structures of two dimeric proteins involved in the His-Asp phosphotransfer systems have been solved. The structure of Spo0B, a *Bacillus subtilis* phosphotransferase, is a unique four-helix bundle that contains a histidine (His 30) at the active site[11]. This His receives a phosphate from Spo0F and transfers it to Spo0A. The structure of the catalytic core of the type II histidine kinase CheA also contains a homodimeric region but lacks the autophosphorylation site[12]. In this case, the substrate His is in the phosphotransfer domain mentioned above. Obviously, His-Asp phosphorelay reactions are diverse in molecular mechanisms, involving a range of different partnerships for their catalysis.

Intra-subunit and inter-subunit surfaces

Despite architectural similarity, helices I and II differ from each other with respect to their structural properties. First, helix I contains many amino acid residues that are highly conserved among members of the histidine kinase family, whereas helix II exhibits significantly lower homology in amino acid sequence (Fig. 2*b*). Second, helix I contains a segment (residues 242–248) that displays structural flexibility, whereas helix II is well-defined and therefore probably more rigid. Interestingly, the flexible segment of helix I contains the most conserved residues: His 243, Thr 247, and Pro 248.

The molecular surface of the four-helix bundle comprises two intra-subunit surfaces, each on the opposite sides of the bundle, and two inter-subunit surfaces, also each on the opposite sides of the bundle (Figs 2*a*, 3*a*). Interestingly, the inter-subunit surface contains two acidic clusters, the first one consisting of Asp 244 from subunit A, Asp 273 and Glu 276 from subunit B, and the second one of Asp 232 and Asp 233 from subunit A, and Asp 286 from subunit B. The first cluster is located in close proximity to His 243, and the second cluster is located near the termini of the molecules. In contrast to the inter-subunit surface, the intra-subunit surface does not possess any major charge characteristics, except for the presence of Arg 246, the only basic residue near the phosphorylation site.

Fig. 4 Summary of mutations in EnvZ domain A. Mutations in domain A that affect EnvZ functions[14,15] are summarized in the space filling model. Mutations that resulted in kinase-/phosphatase+ are colored in green, and kinase+/phosphatase- in light blue. The two subunits are colored in pink and yellow as in Fig. 1. The inter-subunit interface is shown in the left hand panel and the intra-subunit interface in the right hand panel.

His 243 is located in the middle of helix I (Fig. 1*b*); its side chain protrudes from the four-helix bundle and is accessible to the EnvZ catalytic domain and the response regulator OmpR. His 243 is situated at the edge of the intra- and inter-subunit surfaces (Figs 2*a*, 3*a*). In addition to the acidic clusters described above, the inter-subunit surface contains a hydrophobic cluster consisting of Met 238, Ala 239, Leu 236, Phe 284, Ile 280, and Ala 279. These charged and hydrophobic clusters in the vicinity of His 243 are probably involved in interactions with the ATP binding domain of EnvZ (domain B)[13] and the N-terminal domain of OmpR.

To gain insight into which region of EnvZ would interact with OmpR, we performed an NMR titration experiment, in which the ^{1}H-^{15}N HSQC spectra of EnvZ domain A were recorded with successive additions of the regulatory domain of OmpR (residues 1–134). During titration, many backbone NH peaks underwent broadening and eventually disappeared below the noise level (Fig. 3*b*). Interestingly, the NH signals experiencing the most significant broadening effect mapped to the base of the four-helix bundle, as in the view shown in Fig. 3*c*. This region contains not only His 243, but also the acidic patch and two conserved residues, Thr 247 and Pro 248.

Correlation with mutagenesis studies

Numerous genetic and site-directed mutagenesis studies on the autophosphorylation domain of EnvZ have been reported[14,15]. The mutations in domain A that affect EnvZ functions are mapped onto the structure and summarized in Fig. 4. Not surprisingly, mutation of the active histidine (His 243) completely abolished the kinase activity and largely eliminated the phosphatase activity (ref. 14 and references therein). A mutation involving Ala 239, located near the active His, also abolished the kinase activity but retained most of the phosphatase activity[16]. Interestingly, many other mutations involving residues in helix I (Gly 240, Val 241, Ser 242, Thr 247, and Pro 248) produced an opposite effect on the activities of EnvZ: full retention of the kinase activity but a drastically reduced phosphatase activity (see ref. 14 for review). Similarly, mutations involving Asp 273 and Gln 283 in helix II; Tyr 287 and Leu 288 in the linker between domains A and B resulted in the same pattern of change as that of the mutations in helix I[15].

In the solution structure, many of the mutations that disrupt function are localized at the inter-subunit surface (Fig. 4), underlining the functional importance of dimer formation by domain A. Furthermore, most of the mutations studied so far involve residues on the top half of the four-helix bundle in the view shown in Fig. 4. However, the NMR titration experiment (Fig. 3*c*) strongly suggests that OmpR approaches from the bottom part of the four-helix bundle. Similar titration experiments with successive additions of a domain B construct (residues 290–450) yielded no apparent effects on the NMR spectra of domain A (data not shown), indicating a weak affinity ($K_a < 10^3$ M) between the two isolated domains. Taken together, positioning the ATP binding site of domain B in close proximity to His 243 may involve a relatively small area of the four-helix bundle, centered at the active His.

Conclusions

The present work provides the structural details of the dimer of the EnvZ cytoplasmic signaling region. The four-helix bundle architecture formed by the domain A homodimer constitutes an essential platform for the reactions involving autophosphorylation, phosphate transfer to OmpR, and phospho-OmpR dephosphorylation. This structure establishes that functionally deleterious mutations in domain A are localized largely to the inter-subunit surface, confirming the importance of dimerization for EnvZ function.

Methods

Sample Preparation. Over expression in *E. coli* strain BL21(DE3) (F-ompT rBmB) and purification of EnvZ domain A (223–289) were performed as described[6]. The N-terminal domain (residues 1–134) of OmpR was over expressed and purified as described[17]. Uniformly ^{15}N- and ^{15}N/^{13}C-labeled protein samples were obtained by bacterial expression in M9 minimal medium containing ^{15}N-ammonium chloride and/or $^{13}C_6$-D-glucose. The protein was dissolved in 95% $^{1}H_2O$/5% $^{2}H_2O$ to a protein concentration of 1 mM in 20 mM sodium phosphate buffer (pH 7.2) with 50 mM KCl, 5 mM $MgCl_2$, 0.5 mM 4-(2-aminoethyl)-benzenesulfonylfluoride hydrochloride (AEBSF), 5 mM perdeuterated dithiothreitol (DTT), and 50 μM sodium azide.

NMR spectroscopy. All NMR experiments were performed at 25 °C on a Varian four-channel UNITY-plus 500 or a UNITY-600 spectrometer equipped with an actively z gradient shielded triple-resonance probe. ^{1}H, ^{15}N and ^{13}C resonance assignments were achieved from the following three-dimensional through-bond heteronuclear correlation experiments (reviewed in ref. 8): HNCO, HNCACB, HCCH-TOCSY (HB)CBCA(CO)NNH, ^{15}N-edited TOCSY-HMQC and H(CCO)NH, C(CO)NH. Signals from N-terminal residues (Met 223, Ala 224, and Ala 225) were not observed in the two-dimensional ^{1}H-^{15}N HSQC and other ^{15}N-edited spectra, suggesting that they have been cleaved off during bacterial expression. The exchange rate of amide protons was estimated from the difference in intensity of ^{1}H-^{15}N HSQC cross peaks in spectra recorded with and without water presaturation[18]. Heteronuclear $^{3}J_{NH\alpha}$ coupling constants were obtained from a three-dimensional HNHA experiment and $^{3}J_{NH\beta}$ coupling constants from HNHB (reviewed in ref. 19). Stereospecific assignments of β-methylene groups were carried out by analyzing NOE patterns between amide and β protons in a three-dimensional ^{15}N-edited NOESY-HMQC spectrum[8]. Stereospecific assignments of Val and Leu methyl groups were obtained by analyzing a two-dimensional ^{1}H-^{13}C CT-HSQC spectrum on a 10% ^{13}C-labeled sample[19]. All data were processed with nmrPipe and nmrDraw programs[20], and analyzed with PIPP and STAPP[21].

Structure calculations. NOE-based distance constraints were obtained from three-dimensional ^{15}N-edited NOESY-HSQC, ^{1}H-^{15}N HMQC-NOESY-HMQC, and simultaneous ^{15}N/^{13}C-edited NOESY-HSQC spectra (reviewed in ref. 8). Intersubunit distance constraints were mainly obtained from a three-dimensional [^{13}C/F_1]-edited [^{13}C/F_3]-filtered HMQC-NOESY spectrum[8] recorded with a sample containing a 1:1 mixture of uniformly ^{15}N/^{13}C-labeled and unlabeled protein samples. All NOEs were grouped into four distance ranges: strong (1.8–2.9 Å), medium (1.8–3.5 Å), weak (1.8–5.0 Å), and very weak (1.8–6.0 Å). Standard pseudo-atom distance corrections[22] were incorporated to account for center averaging. An additional 0.5 Å was added to the upper distance limits for NOEs involving methyl protons.

Backbone ϕ angle constraints were deduced from the values of $^{3}J_{NH\alpha}$ (ref. 19). For residues with $^{3}J_{NH\alpha}$ <5 Hz, ϕ was restrained to -50° ± 40° and for residues with $^{3}J_{NH\alpha}$ >7 Hz, ϕ was restrained to -120° ± 40°. Backbone φ angle constraints (-50° ± 50°) were included only for those residues within regular α-helical conformation, which was confirmed by $^{13}C\alpha$ and $^{13}C\beta$ chemical shift indices[23].

Structure calculations were performed using a simulated annealing protocol[24] with non-crystallographic symmetry restraints[25] within X-PLOR V3.1 (ref. 26). Hydrogen bonds were added only for residues with slowly exchanging amide protons. The distance restraints are summarized in Table 1. Thirty structures with the lowest total energy were selected out of the 60 calculated structures.

Structure figures were generated using MOLMOL[27] (Fig. 1*a*), Quanta (Fig. 3*c*) from Molecular Simulations Inc., GRASP[28] (Fig. 3*a*), or Molscript[29] and Raster3D[30] (Figs 1*b* and 4). Electrostatic calculations were performed with GRASP[28]. Helical wheel representation was generated using PROTEAN from DNASTAR Inc. (Fig. 2*a*).

Coordinates. Atomic coordinates have been deposited in the Protein Data Bank (accession code 1JOY).

Table 1 Structural statistics of the 30 structures of EnvZ domain A (223–289)[1]

R.m.s. deviations from experimental distance restraints (Å)	
All (1,797)	0.049 ± 0.003
Interresidue sequential (|i - j| = 1) (480)	0.042 ± 0.003
Interresidue short range (1 < |i - j| ≤ 5) (512)	0.059 ± 0.009
Interresidue long range (|i - j| > 5) (46)	0.070 ± 0.004
Intraresidue (632)	0.036 ± 0.005
Hydrogen bond (100)	
0.055 ± 0.004	
Intersubunit (27)	0.090 ± 0.004
R.m.s. deviations from experimental dihedral restraints (°) (168)	0.60 ± 0.096
R.m.s. deviations from idealized covalent geometry	
Bonds (Å)	0.006 ± 0.0001
Angles (°)	0.66 ± 0.014
Impropers (°)	0.41 ± 0.012
Energies (kcal mol^{-1})	
F_{NOE}[2]	213.9 ± 35.4
F_{cdih}[2]	3.62 ± 1.01
F_{repel}[3]	46.1 ± 7.1
E_{L-J}[4]	-100.7 ± 36.4
Average r.m.s. difference (Å)[5]	
Homodimer: Residues in helix I (235–255) and helix II (268–280)	1.10 (1.90)
One subunit: Residues in helix I (235–255) and helix II (268–280)	0.92 (1.80)
Residues in helix I (235–255)	0.82 (1.66)
Residues in helix II (268–280)	0.56 (1.54)
PROCHECK Ramachandran map analysis	
Most favored regions	77.5 ± 2.8%
Additional allowed regions	19.0 ± 3.5%
Generously allowed regions	3.2 ± 2.6%
Disallowed regions	0.2 ± 0.6%

[1]The number of each type of restraints used in the structure calculation is given in parentheses.
[2]F_{NOE} and F_{cdih} were calculated using force constants of 50 kcal mol^{-1} Å^{-2} and 200 kcal mol^{-1} rad^{-2}, respectively.
[3]F_{repel} was calculated using a final value of 4.0 kcal mol^{-1} Å^{-4} with the van der Waals hard sphere radii set to 0.75 × those in the parameter set PARALLHSA supplied with X-PLOR[26].
[4]E_{L-J} is the Lennard-Jones van der Waals energy calculated with the CHARMM empirical energy function and is not included in the target function for simulated annealing calculation.
[5]The average pairwise r.m.s differences are given for selected residues. The value for backbone atoms (N, Ca, and C') is followed by that for all heavy atoms in parenthesis.

Acknowledgments
We thank L. Kay for providing NMR pulse sequences, D. Garrett for helpful instructions on PIPP/STAPP, M. Osawa for providing software used in structure calculation, K. Yap for calculation of interhelical angles, and S. Bagby for critical reading of the manuscript. This work was supported by grants to T.T. from JSPS, to M. Inouye from the NIH, and to M. Ikura from the Howard Hughes Medical Institute. R.I. and D.L. acknowledge HFSP postdoctoral fellowships, and C.T. a postgraduate fellowship from the Ministry of Education, Science and Culture of Japan and from the TARA, University of Tsukuba. M. Ikura is an HHMI International Research Scholar and a Medical Research Council of Canada Scientist.

Correspondence should be addressed to M. Ikura. *email: mikura@oci.utoronto.ca* or M. Inouye *email: inouye@rwja.umdnj.edu*

Received 15 January, 1999; accepted 13 April, 1999.

1. Egger, L.A., Park, H. & Inouye, M. *Genes Cells* **2**, 167–184 (1997).
2. Mizuno, T. *J. Biochem. (Tokyo)* **123**, 555–563 (1998).
3. Swanson, R.V., Alex, L.A. & Simon, M.I. *Trends Biochem. Sci.* **19**, 485–490 (1994).
4. Forst, S., Comeau, D., Norioka, S. & Inouye, M. *J. Biol. Chem.* **262**, 16433–16438 (1987).
5. Forst, S.A. & Roberts, D.L. *Res. Microbiol.* **145**, 363–373 (1994).
6. Park, H., Saha, S.K. & Inouye, M. *Proc. Natl. Acad. Sci. USA* **95**, 6728–6732 (1998).
7. Hidaka, Y., Park, H. & Inouye, M. *FEBS Lett.* **400**, 238–242 (1997).
8. Kay, L.E. *Prog. Biophys. Mol. Biol.* **63**, 277–299 (1995).
9. Zhou, H., Lowry, D.F., Swanson, R.V., Simon, M.I. & Dahlquist, F.W. *Biochemistry* **34**, 13858–13870 (1995).
10. Kato, M., Mizuno, T., Shimizu, T. & Hakoshima, T. *Cell* **88**, 717–723 (1997).
11. Varughese, K.I., Madhusudan, Zhou, X.Z., Whiteley, J.M. & Hoch, J.A. *Mol. Cell* **2**, 485–493 (1998).
12. Bilwes, A.M., Alex, L.A., Crane, B.R. & Simon, M.I. *Cell* **96**, 131–141 (1999).
13. Tanaka, T. *et al. Nature* **396**, 88–92 (1998).
14. Hsing, W. & Silhavy, T.J. *J. Bacteriol.* **179**, 3729–3735 (1997).
15. Hsing, W., Russo, F.D., Bernd, K.K. & Silhavy, T.J. *J. Bacteriol.* **180**, 4538–4546 (1998).
16. Russo, F.D. & Silhavy, T.J. *J. Mol. Biol.* **222**, 567–580 (1991).
17. Delgado, J., Forst, S., Harlocker, S. & Inouye, M. *Mol. Microbiol.* **10**, 1037–1047 (1993).
18. Spera, S., Ikura, M. & Bax, A. *J. Biomol. NMR* **1**, 155–165 (1991).
19. Bax, A. *et al. Methods Enzymol* **239**, 79–105 (1994).
20. Delaglio, F. *et al. J. Biomol. NMR* **6**, 277–293 (1995).
21. Garrett, D.S., Powers, R., Gronenborn, A. & Clore, G.M. *J. Magn. Reson.* **95**, 214–220 (1991).
22. Wüthrich, K., Billeter, M. & Braun, W. *J. Mol. Biol.* **169**, 949–961 (1983).
23. Venters, R.A., Farmer II, B.T., Fierke, C.A. & Spicer, L.D. *J. Mol. Biol.* **264**, 1101–1116 (1996).
24. Nilges, M., Clore, G.M. & Gronenborn, A.M. *FEBS Lett.* **229**, 317–324 (1988).
25. Nilges, M. *J. Mol. Biol.* **245**, 645–660 (1995).
26. Brünger, A.T. *X-PLOR Version3.1: A system for X-ray crystallography and NMR* (Yale University Press, New Haven, Connecticut; 1993).
27. Koradi, R., Billeter, M. & Wüthrich, K. *J. Mol. Graph.* **14**, 51-55, 29–32 (1996).
28. Nicholls, A., Sharp, K.A. & Honig, B. *Proteins Struct. Funct. Genet.* **11**, 281-296 (1991).
29. Kraulis, P. *J. Appl. Crystallogr.* **24**, 946–950 (1991).
30. Merritt, E.A. & Bacon, D.J. *Methods Enzymol.* **277**, 505–524 (1997).
31. Zhang, Z. *et al. Nucleic. Acids Res.* **26**, 3986–3990 (1998).